BIOCHEMISTRY
including biophysical chemistry & molecular biology
Article

Biochemistry **2009,** *48,* 11825–11830 11825
DOI: 10.1021/bi901585q

Distinguishing between Smooth and Rough Free Energy Barriers in Protein Folding†

Stefano Gianni,‡ Maurizio Brunori,*,‡ Per Jemth,§ Mikael Oliveberg,∥ and Mingjie Zhang⊥

‡*Istituto Pasteur-Fondazione Cenci Bolognetti and Istituto di Biologia e Patologia Molecolari del CNR, Dipartimento di Scienze Biochimiche "A. Rossi Fanelli", Università di Roma "La Sapienza", Rome, Italy,* §*Department of Medical Biochemistry and Microbiology, Uppsala University, BMC Box 582, SE-75123 Uppsala, Sweden,* ∥*Department of Biochemistry and Biophysics, Arrhenius Laboratories of Natural Sciences, Stockholm University, S-106 91 Stockholm, Sweden, and* ⊥*Department of Biochemistry, Molecular Neuroscience Center, Hong Kong University of Science and Technology, Clear Water Bay, Kowloon, Hong Kong*

Received September 10, 2009; Revised Manuscript Received October 30, 2009

ABSTRACT: Analysis of curved chevron plots is a powerful tool in investigating protein folding pathways, as the curvatures can be used to gain information about both early and late folding events. When and if accumulation of low-energy intermediates can be ruled out, two different models have classically been applied to describe curved chevron plots, namely , (i) Hammond effects along smooth barrier profiles and (ii) changes in the rate-limiting step between two discrete transition states. The two models lead to very similar numerical solutions, which are generally indistinguishable. This is not surprising, since the smooth barrier assumption approximates barrier profiles with a more complex topology involving multiple local maxima that are too close, or too broad, to yield clear-cut kinks in the chevron data. In this work, we have reconstructed the transition state shifts as a function of protein stability over a wide stability range for three small globular proteins, to screen for fingerprints more sensitive for different barrier profiles. We show that such an analysis represents a valuable test for the discrimination between the two different scenarios.

A typical feature of small single-domain proteins is the ability to fold via an all-or-none reaction. Hence, in the absence of populated intermediates, experimentalists have focused on the characterization of the folding transition state (TS),[1] the highest free energy point on the reaction pathway (*1*). Despite the inherent complexity of the protein folding reaction, the TS is often surprisingly robust and maintains its structural features when its stability is altered by mutagenesis, or solvent conditions (*2*, *3*). However, some protein systems have been reported to display plastic folding pathways characterized by a malleable TS and a broad energy barrier (*4*−*6*). In spite of the remarkable conceptual differences invoked by mechanisms implying either a malleable or a robust TS, it is to date extremely difficult, if not impossible, to unequivocally discriminate between the two models (*7*). This is not surprising, because these two models depict extreme manifestations of a more complex scenario, whereby folding is characterized by a rough energy landscape (*8*). Experimentally, such a roughness may give rise to detectable transition state movements (*9*) or multiple folding pathways (*10*).

It has been empirically observed that changes in folding free energy are linearly related to denaturant concentration, and the slope of this dependence ($m_{D-N} = \delta\Delta G/\delta$[denaturant]) is correlated with the change in accessible surface area upon unfolding (*11*). Since denaturants reduce the stability of the different conformational states according to the degree of their respective solvent-exposed surface area, the activation energy will also be linearly dependent on denaturant concentration. For a simple two-state system, observed kinetics is governed by the sum of the forward and reverse reactions ($k_{obs} = k_F + k_U$). Accordingly, two-state proteins, displaying robust TS, are expected to conform to a perfectly V-shaped dependence of the logarithm of the observed rate constants on denaturant concentration (chevron plot), with linear folding and unfolding arms (Figure 1a) (*3*). Deviations from linearity of the folding and/or unfolding arms result from different scenarios, including (i) accumulation of (un)folding intermediates (Figure 1b) (*12*−*14*), (ii) changes in the rate-limiting step between two discrete barriers (Figure 1c) (*15*, *16*), and (iii) structural changes in TS involving Hammond effects on smooth energy barriers (Figure 1d) (*4*, *17*). Thus, analysis of nonlinear chevron plots is potentially a powerful tool for addressing the shape of folding free energy barriers. While it is sometimes possible to detect the accumulation of low-energy intermediates [i.e., by observing multiphasic kinetics and/or by analyzing the time zero/time infinite fluorescence levels of observed time courses (see, for example, refs *12* and *18*−*20*)], the mechanisms involving either a change in the rate-limiting step (i.e., involving a high-energy intermediate) or smooth energy barriers are often kinetically equivalent (*21*). In this work, we propose a kinetic test to distinguish between the two latter analytical models, based on the assumption that they represent extreme manifestations of the folding energy barrier profile, whereby transition states become experimentally distinguishable only when they are clearly separated along the reaction coordinate. In this context, the smooth barrier formalism represents a low-resolution analysis of a barrier having a more complex profile, involving multiple local maxima that are too close, or too broad, to be distinguished.

The test is applied to two different proteins displaying curved chevron plots: (i) the second PDZ domain from PTP-BL (PDZ2)

†Work partially supported by grants from the Italian Ministero dell'Istruzione dell'Università e della Ricerca (2007B57EAB_004, 20074TJ3ZB_005, and RBRN07BMCT_007) and by the Swedish Research Council.

*To whom correspondence should be addressed: Dipartimento di Scienze Biochimiche "A. Rossi Fanelli", Università di Roma "La Sapienza", P.le A. Moro, 5 00185 Rome, Italy. Phone: +39 06 4450291. Fax: +39 06 4440062. E-mail: maurizio.brunori@uniroma1.it.

[1]Abbreviations: TS, transition state; PDZ, postsynaptic density-95/discs large/zonula occludens-1; PH, pleckstrin homology domain.

Published on Web 10/30/2009

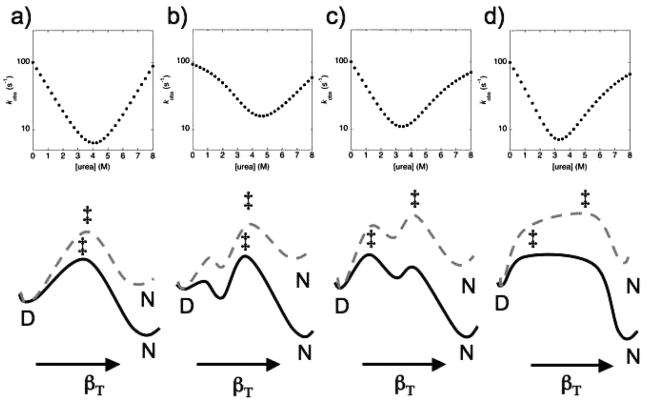

FIGURE 1: Chevron plots and schematic free energy diagrams predicted for (a) two-state folding, (b) three-state folding involving a low-energy accumulated intermediate, (c) three-state folding involving a high-energy never accumulating intermediate, and (d) the smooth barrier models. Solid black lines and dashed gray lines represent schematic energy diagrams for the four different scenarios obtained at low and high denaturant concentrations, respectively. It may be noted that, while two-state folding is expected to result in perfectly V-shaped chevron plots, all the other scenarios return curved chevrons. While the mechanisms involving a change in the rate-limiting step (c) or smooth barrier (d) are generally indistinguishable, accumulation of a folding intermediate (b) results in double-exponential time courses and may be addressed using ultrafast mixing/relaxation techniques (*18*, *19*, *31*).

and (ii) the reconstituted pleckstrin homology domain from PLC-γ (PH), which according to the analysis reported below conform to the two different mechanisms. Moreover, we compare the folding pathway of PDZ2 to that of R16, previously characterized by Clarke and co-workers (*7*, *21*). While the two proteins exhibit similar chevron plots, involving in both cases a rollover in the unfolding branch, the analysis presented below highlights substantial differences in their folding pathways and suggests that, while PDZ2 involves a high-energy intermediate, the pathway of R16 is better described by the smooth barrier model.

EXPERIMENTAL PROCEDURES

Site-directed mutants were produced using a QuikChange site-directed mutagenesis kit (Stratagene). Proteins were expressed and purified as described previously (*22*, *23*). The following buffers were used: 50 mM sodium phosphate from pH 8.0 to 6.3, 50 mM sodium acetate from pH 5.5 to 3.8, and 50 mM sodium formate from pH 3.4 to 2.1. All reagents were of analytical grade.

Stopped-Flow Experiments. Experiments were conducted on an Applied Photophysics (Leatherhead, U.K.) Pi-star stopped-flow instrument; the excitation wavelength was 280 nm, and the fluorescence emission was measured using a 320 nm cutoff glass filter in the case of PDZ2 or using a 360 nm cutoff glass filter in the case of the PH domain. In all experiments, refolding and unfolding were initiated by an 11-fold dilution of the denatured or native protein with the appropriate buffer. Final protein concentrations were typically 1 μM. The observed kinetics were always independent of protein concentration (from 0.5 to 10 μM), as expected from monomolecular reactions without effects due to transient aggregation (*24*). Over and above minor phases due to proline cis−trans isomerization events, observed kinetics were satisfactorily fitted to a single-exponential time course. Each trace was the average of at least five independent shots. Analysis was performed by nonlinear least-squares fitting using the program provided in the Applied Photophysics software. The chevron plots obtained by plotting the observed rate constants versus denaturant concentrations were analyzed as described in the text using either Kaleidagraph (Synergy Software) or Prism (Graphpad).

RESULTS AND DISCUSSION

Analysis of the β_T Dependence on Protein Stability as a test for Assessing the Shape of Folding Free Energy Barriers. A very useful parameter in analyzing the nature of a protein folding transition state is the Tanford β value (β_T), an estimate of the degree of buried surface exposure in the transition state for unfolding relative to the denatured and native states. In particular, the denaturant sensitivity of TS stability relative to those of the denatured (D) and native (N) states is calculated by comparing the denaturant dependence of the folding rate constant [$\delta \ln(k_F)/\delta$[denaturant]] with that of the equilibrium constant [$\delta \ln(K_{D-N})/\delta$[denaturant]].

Both the two-transition state and smooth barrier models will yield changes in β_T as a function of denaturant concentration. Following the smooth barrier model, folding takes place at a nearly iso-energetic level along the barrier profile (*25*). Upon addition of denaturant, the TSs closer in structure to the native state are destabilized to a greater extent than those closer to the denatured state (Hammond effect) (*26*). This has the effect of shifting the highest point in the broad transition state ensemble toward the native state (Figure 1d), resulting in a linear dependence of β_T as a function of denaturant concentration and symmetrical chevron plots. It should be noted that the smooth barrier model also represents an approximation of barrier profiles having complex shapes, e.g., involving multiple local maxima that are too close, or too broad, to be detected. In these cases, the data need to be fitted with a low-resolution model that assumes continuous movement of the transition state ensemble along a smooth barrier top. Under such conditions, the logarithm of the microscopic rate constants for the folding (k_F) and unfolding (k_U) reactions displays a quadratic dependence on denaturant concentration:

$$\ln k_F = \ln k_F^w + m_F[\text{denaturant}] + m_F'[\text{denaturant}]^2 \quad (1)$$

$$\ln k_U = \ln k_U^w + m_U[\text{denaturant}] + m_U'[\text{denaturant}]^2 \quad (2)$$

$$k_{obs} = k_F^w e^{(m_F[\text{denaturant}]+m'[\text{denaturant}]^2)} + k_U^w e^{(m_U[\text{denaturant}]+m'[\text{denaturant}]^2)} \quad (3)$$

where k_F and k_U are the folding and unfolding rate constants, respectively, k_F^w and k_U^w are the folding and unfolding rate constants in the absence of denaturant, respectively, and m_F and m_F' (folding) and m_U and m_U' (unfolding) define their respective dependence on denaturant concentration.

Furthermore, it follows from the two-state and linear free energy dependence assumptions that curvature of the folding and unfolding arms will be symmetrical (*4*):

$$\frac{\partial \partial G_{i \to j}}{\partial [\text{denaturant}]^2} = 0 \quad (4)$$

$$m_F' = m_U' \quad (5)$$

Hence the value of β_T may be calculated as a function of denaturant concentration as follows:

$$\frac{\partial \ln k_F}{\partial[\text{denaturant}]} = 2m_F'[\text{denaturant}] + m_F \quad (6)$$

$$\frac{\partial \ln K_{D-N}}{\partial[\text{denaturant}]} = \frac{m_{D-N}}{RT} \quad (7)$$

$$\beta_T = RT\frac{2m_F'[\text{denaturant}] + m_F}{m_{D-N}} \quad (8)$$

where, as described in the introductory section, $m_{D-N} = \delta\Delta G/\delta[\text{denaturant}]$ and is correlated to the change in accessible surface area upon unfolding (*11*).

On the other hand, according to the two-transition state model, the folding TSs are treated as fixed on the reaction coordinate, with curvatures in the chevron plot arising from a switch between discrete transition states separated by one or more obligatory on-pathway high-energy intermediates (*27*, *28*). Under such conditions, a curvature may be observed in only one limb of a chevron plot. By considering a chevron plot displaying an unfolding rollover, it can be stated that

$$\ln k_F = \ln k_F^w + m_F[\text{denaturant}] \quad (9)$$

$$\ln k_U = \ln k_U^w + m_U[\text{denaturant}] - \ln(1 + K_{part}e^{m_{part}[\text{denaturant}]}) \quad (10)$$

where K_{part} is the apparent partition factor between the two transition states and m_{part} its associated m value.

The two-transition state model implies discrete shifts between well-separated transition states along the barrier profile, which should manifest as distinct "kinks" in the chevron plots. In an effort to test whether curve fitting of individual chevron plots could be used to distinguish clear kinks from continuous movements along a smooth barrier, we simulated different chevron plots involving two distinct maxima at different β_T values (with a $\Delta\beta_T$ of up to 0.6) and fitted them with the smooth barrier equation (data not shown). We observed that, for a protein containing 100 amino acids (i.e., corresponding to an m_{D-N} of 1.5 kcal mol^{-1} M^{-1} in urea), an experimental error on k_{obs} as small as 5% is sufficient to mask any systematic deviation from residual analysis. This is not surprising since, as shown by Scott and Clarke, the two models are basically indistinguishable even when challenged with extensive site-directed mutagenesis (*21*).

For the two-transition state model, the β_T may be calculated as a function of denaturant concentration by subtracting from unity the derivative of the logarithm of the unfolding rate constant normalized by the total m_{D-N} value:

$$\frac{\partial \ln k_U}{\partial[\text{denaturant}]} = m_U - \frac{m_{part}K_{part}e^{m_{part}[\text{denaturant}]}}{1 + K_{part}e^{m_{part}[\text{denaturant}]}} \quad (11)$$

$$\beta_T = 1 - RT\left(\frac{m_U}{m_{D-N}} - \frac{1}{m_{D-N}}\frac{m_{part}K_{part}e^{m_{part}[\text{denaturant}]}}{1 + K_{part}e^{m_{part}[\text{denaturant}]}}\right) \quad (12)$$

The β_T is thus expected to display a sigmoidal dependence on denaturant concentration (*29*), with at least two limiting β_T values, reflecting the relative change in accessible surface area between discrete transition states; the apparent midpoint of the β_T versus [denaturant] plot reflects the experimental condition under which the two TSs are at isostability (i.e., $K_{part} = 1$). Since the smooth barrier model would be characterized by a linear dependence of β_T on denaturant concentration (or protein stability), a rigorous analysis should allow unequivocal distinction between two-transition states and smooth free energy barriers. However, such a task is complicated by the reversible nature of the folding reaction, which implies observed kinetics to be governed by a combination of folding and unfolding microscopic rate constants. For example, a direct measurement of the folding rate constants at higher denaturant concentrations is prevented, since the process is dominated by the unfolding rate constant. This implies that the two models are kinetically indistinguishable from analysis of individual chevron plots, the region close to the denaturation midpoint being the only interval where information about both the folding and unfolding rate constants, and thus the curvature of the folding and unfolding arms, can be obtained.

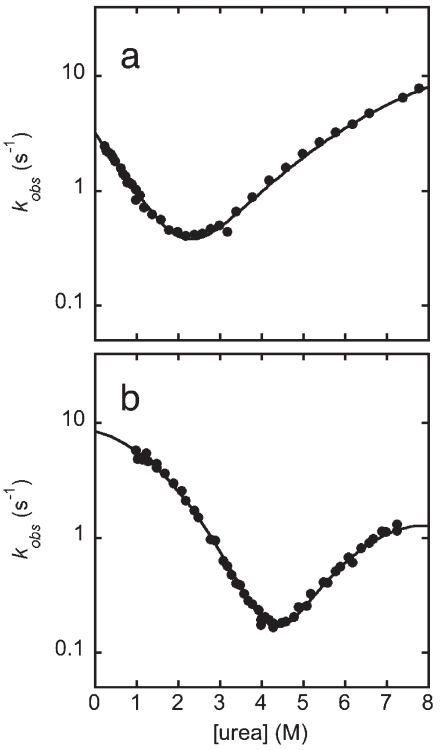

FIGURE 2: Chevron plot of PDZ2 (a) and PH (b) domains measured in the presence of 50 mM sodium phosphate buffer (pH 7.0) at 25 °C. The line is the best fit to eq 3. As described in the text, it was impossible to discriminate between the smooth and two-transition state barriers by comparing curve fitting residuals of individual chevron plots.

In this study, we present a method for circumventing this limitation. To enhance the resolution of the characterization of free energy barriers, we calculate the shape of the β_T versus stability profile, by measuring the chevron plots under a variety of solvent conditions. In particular, by measuring the folding−unfolding kinetics of a given protein (wild type and point mutants) while altering its stability using different pH conditions and/or in the presence or absence of stabilizing salts (such as sodium sulfate), we should be able to monitor the β_T versus stability dependence over a wide protein stability range. We then compared the obtained profiles with the dependencies expected from the two-transition state (sigmoidal) versus smooth (linear) barrier models.

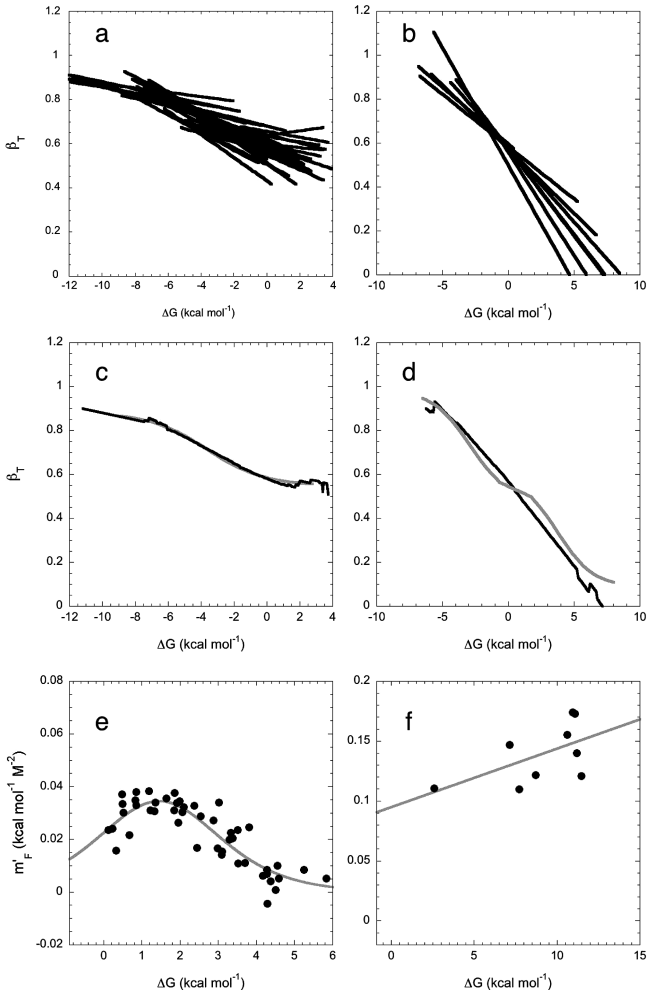

FIGURE 3: Dependence of β_T vs stability for the PDZ and PH domains. Different chevron plots of the PDZ2 (a) and PH (b) domains were fitted to eq 3. From fitting parameters, we reconstructed the linear β_T vs stability profile of each chevron plot by employing eq 8 (reported as black lines). Data refer to folding or unfolding conducted under different pH conditions (ranging from 2.7 to 8) and in the presence or absence of sodium sulfate (maximum concentration of 0.4 M). In the case of the PDZ2 domain, we also included data referring to the conservative site-directed mutants reported in ref *32*. A similar behavior was observed when the mutants were not included in the analysis (data not shown). (c and d) Averaged β_T vs stability dependence for the PDZ2 (c) and PH (d) domains. The gray line represents the β_T calculated according to the multiple-transition state model, as formalized in eq 12. (e and f) m'_F values for PDZ2 (e) and PH (f) domains at different unfolding stabilities. While in the case of the PDZ2 domain (e) data could be satisfactorily fitted to eq 15, as expected if a change in the rate-limiting step were operative, PH domain data could not be fitted. Hence, a linear fit has been reported in panel f to guide the eye.

Comparing the Folding Kinetics of PDZ2 and PH Domains. We performed a complete characterization of two different proteins displaying curved chevron plots [PDZ2 and PH domains (Figure 2)]. Over and above slow phases due to proline cis−trans isomerization (data not shown), folding and unfolding kinetics were well-fitted to single-exponential time courses, and no additional fast phases could be detected, indicating the absence of low-energy accumulated intermediates. In the case of the PDZ2 domain, we previously excluded the presence of low-energy intermediates also by ligand-induced folding experiments (*30*).

The chevron plots of both PDZ2 and PH domains measured at pH 7.0 and 25 °C can be adequately fitted to both the smooth and two-transition state models [the latter involving two on-pathway intermediates in the case of the PH domain (Figure 2)]. Furthermore, in all cases, thermodynamic parameters obtained from equilibrium denaturations were consistent, within experimental error, with data obtained by fitting the chevron plots to the two different kinetic models (data not shown). Hence, as previously shown for other protein systems (*21*), a comparison of the fit to the smooth and two-transition state models of individual chevron plots does not allow us to distinguish between the two different scenarios.

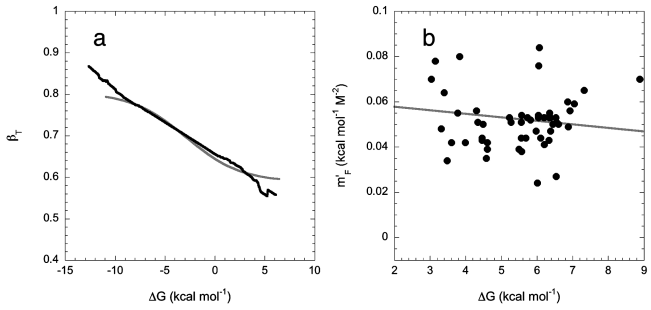

FIGURE 4: Dependence of β_T vs stability for R16. (a) Averaged β_T vs stability dependence for R16. Data refer to the site-directed variants reported in refs *7* and *21*. The gray line represents the β_T values calculated according to the two-transition state model, as formalized in eq 12. (b) m'_F values for R16 at different unfolding stabilities. Data could not be fitted to eq 15; hence, a linear fit is reported to guide the eye.

The folding and unfolding kinetics of a simple two-state protein, characterized by a robust transition state, can be described as follows:

$$k_{obs} = k_F^w e^{(-m_F[\text{denaturant}])} + k_U^w e^{(m_U[\text{denaturant}])} \quad (13)$$

where k_F and k_U are the folding and unfolding rate constants, respectively, m_F and m_U are their associated m values, and k_F^w and k_U^w represent the folding and unfolding rate constants in the absence of denaturant, respectively.

Upon comparison of eqs 3 and 13, it may be noted that the smooth barrier model (malleable TS) will resemble the simple two-state model (robust TS) at the limiting condition of m'_F approaching zero. Hence, the m'_F value reflects the degree of curvature of a chevron plot and may be thus used empirically to estimate the variations in β_T. In particular, when a chevron plot is fit to eq 3, the estimated m'_F will in turn be a measure of the overall change in β_T value within the stability window experimentally explored in the chevron (see eq 8). Following these premises, in an effort to distinguish between the broad and two-transition state barrier models, we resorted to reconstructing empirically the dependence of β_T over a wide window of protein stability. Thus, we analyzed the chevron plots of the two proteins, as obtained under a variety of different experimental conditions.

After fitting each individual chevron plot of PDZ2 and PH domains to eq 3, we calculated the β_T versus stability profile for each individual chevron and obtained a family of lines spanning a wide protein stability range for each of the two proteins (Figure 3a,b). Although each individual chevron was fitted with a bias for a linear dependence of β_T versus stability (as formalized in eq 8), a different behavior was observed for the two proteins. Qualitatively, while in the case of the PH domain it appears that the different lines display a common interception at $\beta_T \approx 0.65$, in the case of the PDZ2 domain, the behavior is more complex.

To analyze quantitatively the overall dependence of β_T versus stability for the two systems, we performed two tests on the different data sets. First, we computed an average of the calculated families of linear profiles for each protein. More specifically, all the lines obtained within a given denaturant concentration window (1−7 M urea) were averaged and compared with the dependence expected from the two-transition state model (Figure 3c,d). Inspection of Figure 3 reveals that, while in the case of the PH domain an average of the different lines returns an approximately linear behavior (Figure 3d), the PDZ2 domain displays a sigmoidal profile (Figure 3c). In the latter case, there was also an excellent agreement between the profile obtained by averaging the lines using the smooth barrier analysis and the profile expected from the two-transition state model. These observations suggested that, in the case of PDZ2, even when the smooth barrier model is applied, a sigmoidal profile could be observed, as expected if a change in the rate-limiting step between two discrete barriers were operative.

A second test for detecting changes in rate-limiting step between two different TSs may be invoked when comparing $\delta\beta_T/\delta$[denaturant] values for the two different models. By taking the derivative of eq 8 (smooth barrier) and eq 12 (two-transition state barrier), we may formalize the following equations.

For the smooth barrier model

$$\frac{\partial\beta_T}{\partial[\text{denaturant}]} = 2RTm_F' \tag{14}$$

For the two-transition state model

$$\frac{\partial\beta_T}{\partial[\text{denaturant}]} = \frac{1}{m_{D-N}} \frac{m_{part}K_{part}e^{m_{part}[\text{denaturant}]}(1 + K_{part}e^{m_{part}[\text{denaturant}]}) - m_{part}K_{part}{}^2e^{2m_{part}[\text{denaturant}]}}{(1+K_{part}e^{m_{part}[\text{denaturant}]})^2} \tag{15}$$

In simple terms, while $\delta\beta_T/\delta$[denaturant] is expected to be constant in the smooth barrier scenario, it will display a bell-shaped function in the two-transition state model, $\delta\beta_T/\delta$[denaturant] tending to zero under the limiting conditions where the protein is infinitely unstable and infinitely stable.

As discussed above, the m_F' value is a measure of the overall change in β_T within the stability window experimentally explored in the chevron and may thus be used to monitor changes in $\delta\beta_T/\delta$[denaturant]. If curvatures in the chevron plot are due to changes in the rate-limiting step, m_F' should display a bell-shaped dependence as a function of protein stability (as formalized in eq 15), which is linearly correlated to denaturant concentration. The calculated m_F' values for the PDZ2 and PH domains at different unfolding stabilities are reported in Figure 3e,f. Strikingly, while in the case of the PH domain m_F' values were found to scatter around an average, a bell-shaped dependence is observed for the PDZ2 domain, with values consistent with eq 15. The bell-shaped dependence clearly indicates that the PDZ2 domain follows the two-transition state model, and that our proposed test is able to distinguish between the two-transition state and smooth barrier models.

In summary, while both PDZ2 and PH domains display curved chevron plots, the kinetic test presented in this work suggests that their associated barriers have different levels of fine structure. Folding of the PDZ2 domain is best described by the two-transition state model and folding of the PH domain by the smooth barrier model. To further validate the proposed test, we subjected previously published data for the R16 protein (*7*, *21*) to the same type of analysis. Importantly, R16 kinetics (i) is reminiscent of that of the PDZ2 domain, i.e., displaying a clear rollover only in the unfolding arm, and (ii) has been characterized extensively by Clarke and colleagues (many chevron plots of site-directed mutants are available).

Also for R16, the β_T versus stability and m_F' versus stability profiles were calculated as described above and reported in Figure 4. It may be noticed that, while individual chevron plots of R16 and its variants are very similar to those of the PDZ2 domain, the former protein is consistent with the behavior expected from the smooth barrier model; i.e., it displays a quasi-linear β_T versus stability profile, and m_F' is insensitive to protein stability. On the basis of these observations, we conclude that the R16 folding pathway is better captured by the smooth barrier scenario.

CONCLUSIONS

By global analysis of the folding and unfolding kinetics measured over a wide range of protein stabilities, we reconstructed a complete β_T versus stability profile of three different small proteins displaying curved chevron plots. Data reveal that while the folding of PDZ2 involves a high-energy intermediate and discrete shifts between distinct maxima, PH domain folding and R16 folding are better described by continuous TS movement over a smooth barrier profile. While the two mechanisms are nearly indistinguishable when the fits are compared to individual chevron plots, the proposed test can successfully discriminate between the two different scenarios.

ACKNOWLEDGMENT

We thank Dr. Jane Clarke (Cambridge, U.K.) for sharing the data of R16 and site-directed mutants.

REFERENCES

1. Fersht, A. R. (2000) Transition-state structure as a unifying basis in protein-folding mechanisms: Contact order, chain topology, stability, and the extended nucleus mechanism. *Proc. Natl. Acad. Sci. U.S.A. 97*, 1525–1529.
2. Itzhaki, L. S., Otzen, D. E., and Fersht, A. R. (1995) The structure of the transition state for folding of chymotrypsin inhibitor 2 analysed by protein engineering methods: Evidence for a nucleation-condensation mechanism for protein folding. *J. Mol. Biol. 254*, 260–288.
3. Jackson, S. E., and Fersht, A. R. (1991) Folding of chymotrypsin inhibitor 2. 1. Evidence for a two-state transition. *Biochemistry 30*, 10428–10435.
4. Ternstrom, T., Mayor, U., Akke, M., and Oliveberg, M. (1999) From snapshot to movie: ϕ analysis of protein folding transition states taken one step further. *Proc. Natl. Acad. Sci. U.S.A. 96*, 14854–14859.
5. Lindberg, M. O., and Oliveberg, M. (2007) Malleability of protein folding pathways: A simple reason for complex behaviour. *Curr. Opin. Struct. Biol. 17*, 21–29.
6. Cellmer, T., Henry, E. R., Kubelka, J., Hofrichter, J., and Eaton, W. A. (2007) Relaxation rate for an ultrafast folding protein is independent of chemical denaturant concentration. *J. Am. Chem. Soc. 129*, 14564–14565.
7. Scott, K. A., Randles, L. G., and Clarke, J. (2004) The folding of spectrin domains II: ϕ-value analysis of R16. *J. Mol. Biol. 344*, 207–211.

8. Hyeon, C., and Thirumalai, D. (2003) Can energy landscape roughness of proteins and RNA be measured by using mechanical unfolding experiments? *Proc. Natl. Acad. Sci. U.S.A. 100*, 10249–10253.
9. Schlierf, M., and Rief, M. (2005) Temperature softening of a protein in single-molecule experiments. *J. Mol. Biol. 354*, 497–503.
10. Hyeon, C., and Thirumalai, D. (2008) Multiple probes are required to explore and control the rugged energy landscape of RNA hairpins. *J. Am. Chem. Soc. 130*, 1538–1539.
11. Myers, J. K., Pace, C. N., and Scholtz, J. M. (1995) Denaturant m values and heat capacity changes: Relation to changes in accessible surface areas of protein unfolding. *Protein Sci. 4*, 2138–2148.
12. Ferguson, N., Capaldi, A. P., James, R., Kleanthous, C., and Radford, S. E. (1999) Rapid folding with and without populated intermediates in the homologous four-helix proteins Im7 and Im9. *J. Mol. Biol. 286*, 1597–1608.
13. Matouschek, A., Kellis, J. T., Jr., Serrano, L., Bycroft, M., and Fersht, A. R. (1990) Transient folding intermediates characterized by protein engineering. *Nature 346*, 440–445.
14. Parker, M. J., Spencer, J., and Clarke, A. R. (1995) An integrated kinetic analysis of intermediates and transition states in protein folding reactions. *J. Mol. Biol. 253*, 771–786.
15. Sanchez, I. E., and Kiefhaber, T. (2003) Evidence for sequential barriers and obligatory intermediates in apparent two-state protein folding. *J. Mol. Biol. 325*, 367–376.
16. Oliveberg, M. (1998) Alternative explanations for multi-state kinetics in protein folding: Transient aggregation and changing transition-state ensembles. *Acc. Chem. Res. 31*, 765–772.
17. Otzen, D. E., Kristensen, O., Proctor, M., and Oliveberg, M. (1999) Structural changes in the transition state of protein folding: Alternative interpretations of curved chevron plots. *Biochemistry 38*, 6499–6511.
18. Capaldi, A. P., Shastry, M. C., Kleanthous, C., Roder, H., and Radford, S. E. (2001) Ultrarapid mixing experiments reveal that Im7 folds via an on-pathway intermediate. *Nat. Struct. Biol. 8*, 68–72.
19. Jemth, P., Gianni, S., Day, R., Li, B., Johnson, C. M., Daggett, V., and Fersht, A. R. (2004) Demonstration of a low-energy on-pathway intermediate in a fast-folding protein by kinetics, protein engineering, and simulation. *Proc. Natl. Acad. Sci. U.S.A. 101*, 6450–6455.
20. Khorasanizadeh, S., Peters, I. D., and Roder, H. (1996) Evidence for a three-state model of protein folding from kinetic analysis of ubiquitin variants with altered core residues. *Nat. Struct. Biol. 3*, 193–205.
21. Scott, K. A., and Clarke, J. (2005) Spectrin R16: Broad energy barrier or sequential transition states? *Protein Sci. 14*, 1617–1629.
22. Gianni, S., Calosci, N., Aelen, J. M., Vuister, G. W., Brunori, M., and Travaglini-Allocatelli, C. (2005) Kinetic folding mechanism of PDZ2 from PTP-BL. *Protein Eng., Des. Sel. 18*, 389–395.
23. Wen, W., Yan, J., and Zhang, M. (2006) Structural characterization of the split pleckstrin homology domain in phospholipase C-γ1 and its interaction with TRPC3. *J. Biol. Chem. 281*, 12060–12068.
24. Silow, M., and Oliveberg, M. (1997) Transient aggregates in protein folding are easily mistaken for folding intermediates. *Proc. Natl. Acad. Sci. U.S.A. 94*, 6084–6086.
25. Oliveberg, M. (2001) Characterisation of the transition states for protein folding: Towards a new level of mechanistic detail in protein engineering analysis. *Curr. Opin. Struct. Biol. 11*, 94–100.
26. Hammond, G. S. (1955) A correlation of reaction rates. *J. Am. Chem. Soc. 77*, 334–339.
27. Bachmann, A., and Kiefhaber, T. (2001) Apparent two-state Tendamistat folding is a sequential process along a defined route. *J. Mol. Biol. 306*, 375–386.
28. Khan, F., Chuang, J. I., Gianni, S., and Fersht, A. R. (2003) The kinetic pathway of folding of barnase. *J. Mol. Biol. 333*, 169–186.
29. Fersht, A. R. (2000) A kinetically significant intermediate in the folding of barnase. *Proc. Natl. Acad. Sci. U.S.A. 97*, 14121–14126.
30. Ivarsson, Y., Travaglini-Allocatelli, C., Jemth, P., Malatesta, F., Brunori, M., and Gianni, S. (2007) An on-pathway intermediate in the folding of a PDZ domain. *J. Biol. Chem. 282*, 8568–8572.
31. Shastry, M. C., Luck, S. D., and Roder, H. (1998) A continuous-flow capillary mixing method to monitor reactions on the microsecond time scale. *Biophys. J. 74*, 2714–2721.
32. Gianni, S., Geierhaas, C. D., Calosci, N., Jemth, P., Vuister, G. W., Travaglini-Allocatelli, C., Vendruscolo, M., and Brunori, M. (2007) A PDZ domain recapitulates a unifying mechanism for protein folding. *Proc. Natl. Acad. Sci. U.S.A. 104*, 128–133.